Islamic Azad University

Journal of
Optoelectronical Nanostructures

Winter 2021 / Vol. 6, No. 1

Research Paper

Design of High Sensitivity and high FoM Refractive Index Biosensor Based on 2D-Photonic Crystal

Mahmood Momeni[1], Mohammad Javadiansarraf [*,1], Farzan Khatib[1]

[1] Department of Electrical Engineering, Mashhad Branch, Islamic Azad University, Mashhad, Iran

Received: 22 Sep. 2021
Revised: 21 Oct. 2021
Accepted: 18 Nov. 2021
Published: 15 Dec. 2021

Use your device to scan and read the article online

Keywords: Basel cell detection biosensor, Finite-difference time domain High figure of merit biosensor, , High sensitivity biosensor, Label free Photonic crystal biosensor, Refractive indexsensor

Abstract: This paper aims at proposing a new design based on the refractive index using 2D photonic crystals (PCs) for diagnosing basal cell carcinoma (BCC). This project consists of a square array of GaAs rods in SiO2. This structure has two inlet and outlet waveguides and a micro-cavity. Waveguides are employed to couple light to the cavity, and the cavity to inject analyte into it. Some PC rods were used to separate the cavity from the inlet and outlet waveguides. The results show that by injecting an analyte into the cavity and changing its refractive index, a shift occurs in the resonance wavelength of the transmission spectrum. The high sensitivity coefficient obtained for this sensor is 730 nm/RIU and its high Figure of Merit (FoM) is 11428. For numerical analysis of the transmission spectrum, Q-factor, and sensor sensitivity, the finite-difference time-domain (FDTD) method was used. High simplicity, sensitivity, FoM make it suitable for biosensing applications.

Citation: Momeni M, Javadian Sarraf M, Khatib F .Design of high sensitivity and high FoM refractive index biosensor based on 2D-photonic crystal.
Journal of Optoelectronical Nanostructures, 2021; 6 (4): 33- 58.
DOI: 10.30495/JOPN.2022.27033.1217

***Corresponding author:** Mohannad Javadiansarraf
Address: Department of Electrical Engineering, Mashhad Branch, Islamic Azad University, Mashhad, Iran. **Tell:** 00989153109755
Email: m.j.sarraf@mshdiau.ac.ir

1. INTRODUCTION

In recent decades, changes in human lifestyle in the form of, for example, mechanization, have created problems for human life. Cancer is one of the problems that people face due to these changes in their lives. It has been growing in recent years. Accordingly, it has incurred heavy costs for the people, increased the mortality rate of human beings, and affected their lives seriously.
If we can diagnose this disease earlier with some methods, in many cases, its spread can be tackled and heavy costs can be prevented. Therefore, designing equipment that can be used to detect cancers is very important. One of the tools that help us diagnose some cancers is photonic crystals (PCs). Since cancer cells are characterized by having a higher protein volume in the large nucleus of the cell, Its refractive index is higher than the refractive index of a healthy cell. Healthy and cancer cells can be distinguished via this index.

PCs are composed of dielectric materials whose refractive index changes alternatively. These alternative changes create a unique feature in PCs. One of the main features of this structure is having the optical bandgap [1] which prevents the passage of light spectra with specific wavelengths through the structure [2]. Whenever there is a defect in such a structure, light of a certain wavelength can be passed through the gap of the band which is the basis of PCs.

In recent decades, many PC-based devices have been made, each of which has solved many problems in the world based on its properties. The design of filters [3-14], multiplexers, comparators, modulators, and sensors [15-21] are some among the others. PCs are also used in other fields, such as defense, food, safety, quality control, aerospace, environment, and security [22, 23]. Structures such as ring resonators [24], micro-cavities [25-29], waveguides, and slot-waveguides [30-32] can be used to design various PC-based devices. PC- based structures can also be used for biosensors so that they can be easily implemented on a semiconductor substrate using integrated circuit technology. This rule makes it easy to integrate PC equipment with electrical equipment. This integration of biosensors on a chip reduces the cost and size of the equipment. Since micro-cavities with coupled waveguides [33-36]offer many advantages in terms of the Q-factor, high sensitivity coefficient, compactness, and parallel measurement[19, 37, 38], and the ease in the development of sensor arrays, this paper seeks to use these advantages in sensor design.
A variety of photonic crystals have been used for refractive index sensing applications. Here are some of the newest and most important examples. Huang et al, have demonstrated a low crosstalk sensor with sensitivity ($\Delta\lambda/\Delta n$) of 134-145.5 nm/ refractive index units (RIU) and the Q-factors of 10000[38]. Shivam et al, have presented a refractive index sensor with an output power of 89.8% [39]. Jindal et al, have presented a bio-

sensing platform based on nano-cavity-coupled PC waveguide for diseased cell detection with high selectivity and high sensitivity for different cancer cells [40]. Ammari et al, have demonstrated a 2D PC biosensor with a sensitivity of 668 nm/RIU and a lower detection limit (DL) of 0.002 RIU [41]. A sensor with a sensitivity of 613nm/RIU has been studied by Shi et al, [18]. Rahman-Zadeh et al, have presented a hybrid PC cavity biosensor with a sensitivity of 300 nm/RIU and Q-factor 418 [42]. Another biosensor with a sensitivity of 425 nm / RIU and DL = 0.001RIU has been designed [33]. Tavousi et al, have presented a biosensor with a sensitivity of 690nm/RIU [43].

Most sensors use dielectric rods in the air or air holes in a dielectric. In this paper, the structure of the sensor consists of GaAs rods inside a dielectric made of SiO2. Also, a hole is made in the center used to inject the analyte and identify its properties.

Due to the advantages of coupled-cavity waveguides, a new 2D- PC structure based on the refractive index was used in this paper. The wavelength shift mechanism of the output spectrum by changing the refractive index of the analyte inside the cavity is the basis of the work of sensors based on refractive index. In other words, by changing the refractive index, the resonance wavelength of the emission spectrum changes.

This paper presents a resonant filter for measuring refractive index changes. One of the applications of this sensor is to detect basal cancer cells. The refractive indices of healthy and cancerous basal cells are 1.36 and 1.38 [17], respectively. Instead of increasing the Q-factor, in this paper, the spatial resonance profile is confined in the cavity, obtains a significant change in the resonance wavelength for a slight change in refractive index. To this end, the sensitivity studied as the most important parameter of the biosensor reaches a high value of 730nm/RIU.

After the introduction in section 1, this article is structured as follows: Section 2 explaines the mechanism of biosensors; Section 3 is devoted to the design of the sensor; optimization of the sensitivity is discused in Section 4. A summary of the results as well as a comparison of this article with other articles is provided in Section 5; the FoM of the sensor is analyzed in Section 6, and the last part is about the onclusion.

2. MECHANISM OF BIOSENSORS

Different structures can be used to design optical filters. These structures are constructed by the material whose refractive index is to be changed is put in a cavity. The light of a specific wavelength is emitted on the structure. After

interaction with the analyte, a wavelength shift proportional to the analyte's refractive index occurs in the spectra. Some of the most common biosensing structures are shown in Fig.1.

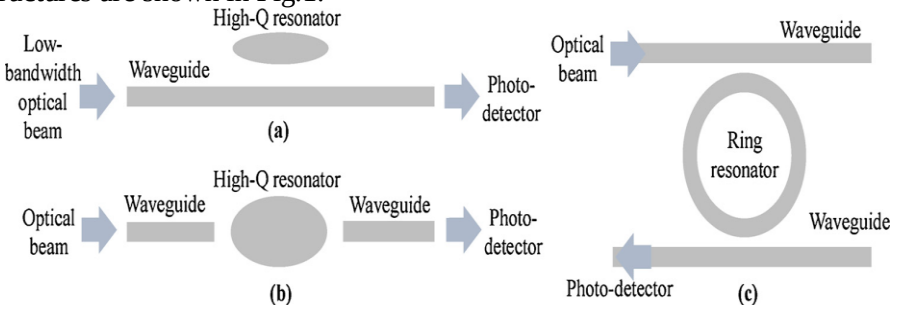

Fig. 1. The most common PC biosensors structures, (a) a cavity side-coupled biosensor, (b) two waveguide couplers-resonator, (c) ring resonator-coupled waveguides biosensors [17]

When the cavity is filled with the analyte, by changing the material's refractive index inside the micro-cavity, a displacement occurs during the resonance wavelength of the transmission spectra. Changing the refractive index of the analyte shifts the optical response of the filter in terms of wavelength according to the perturbance theory, calculated via the following equation [44].

$$\frac{\Delta\omega}{\omega_{res}} = \frac{\iiint_v (\delta\mu\, H_r^2 + \delta\varepsilon\, E_r^2)dv}{\iiint_v (\mu\, H_r^2 + \varepsilon\, E_r^2)dv}$$

$$= -\frac{1}{W}\iiint_v \left(\frac{\delta\varepsilon}{\varepsilon}.We + \frac{\delta\mu}{\mu}.Wm\right)dv \quad (1)$$

In which ε and μ are, permittivity and permeability and Hr and Er show the magnetic and electric field respectively, W is of the whole energy stored in micro-cavity, Wm and We are the densities of magnetic and electric energy respectively. The formula can be changed due to only the permittivity changes, so:

$$\frac{\Delta\omega}{\omega_{res}} = -\frac{1}{W}\iiint_v \left(\frac{\delta\varepsilon}{\varepsilon}.We\right)dv =$$
$$-\frac{1}{W}\iiint_v (\delta\varepsilon_r\ \varepsilon_0.E_r^2)dv$$

(2)

In which ε_0 is the permittivity of free space and, ε_r, μ_r are relative permittivity and relative permeability respectively. We know, $n=\sqrt{\varepsilon_r\mu_r}$

n is the analyte refractive index.

So, the optical shift-induced (Δω) can be approximated by (3)) [45].

$$\frac{\Delta\omega}{\omega res}=-\sigma\frac{\delta n}{n} \quad (3)$$

In which δn is refractive index change Where σ is the optical overlap integral or the filling factor, that indicates the value of the shift due to perturbation in PC biosensor, that is infiltrated with the analyte, leads to perturbation. And σ is dependent on the Part of the resonant energy stored in a place where the refractive index alters. It is attempted to maximize Δω for a certain δn.

If the spectrum of the sensor is very sharp, minimum variation in sensor parameters leads to a whole failure.

The Q-factor and the sensitivity coefficient are obtained from the following equation. as:

$$S_n(\lambda)=\frac{\partial\lambda_{res}}{\partial n_{analyte}}\approx\frac{\Delta\lambda}{\delta n}\ \text{(nm/RIU)} \quad (4)$$

$$Q=\frac{\lambda_{res}}{\Delta\lambda FWHM} \quad (5)$$

Where, λ_{res} is the resonance wavelength and Δλ is the resonance wavelength shift and $\Delta\lambda_{FWHM}$ is the full width at half maximum.

In a resonator where a photon is confined in a nanoscale region where the waves are constructively interfering, the effective interaction length can be enhanced by increasing the Q-factor of the resonant mechanism. The Q-factor is defined as [41].

$$Q=-\frac{U(t)\omega 0}{(dU(t))/dt} \quad (6)$$

Where U(t) is the total energy of the confined light field and $\frac{-\omega 0}{(dU(t))/dt}$ is proportional to the energy losses per electromagnetic oscillation.

We have $U(t)\propto E(t)^2$. From the above equation,

$$E(t)=e^{\frac{-\omega_0 t}{2Q}}e^{(-j\omega|t|)} \quad (7)$$

And according to Fourier transform.

$$E(t)=\frac{1}{\sqrt{2\pi}}\int_{-\infty}^{\infty}E(\omega)e^{-j\omega t}d(\omega) \quad (8)$$

A spectral response that indicates a Lorentzian line is expected:

$$|E(\omega)|^2\propto\frac{1}{(\omega-\omega_0)^2-(\frac{\omega_0}{2Q})^2} \quad (9)$$

Where ω_0 is the resonance frequency and $\Delta\omega=\frac{\omega_0}{Q}$ is FWHM. The total intrinsic Q-factor is [38]:

$$\frac{1}{Q_{total}}=\frac{1}{Q_a}+\frac{1}{Q_s}+\frac{1}{Q_r} \quad (10)$$

Where $1/Q_a$ represents losses of the photon by material absorption and $1/Q_s$ denotes scattering losses due to surface defects or surface inhomogeneous, and $1/Q_r$ shows radiative losses.

The FoM can be defined as FoM = S · Q/λres [42]. However, the trade-off between S and Q limits the FoM. To achieve high S, Some designs focused on donor and acceptor modes some others increased the cavity length resulting in increasing Q-factor that allows smaller changes in refractive index to be detected. The high Q increases the interaction time between light and analyte, while the larger mode volume results in a larger fill fraction, both factors resulting in higher sensitivity. High overlap of the analyte with light causes S to increase.

In this paper, to calculate the photonic band structure, the plane wave expansion (PWE) [46, 47], and to determine the transmission spectra behavior of the Maxwell equations [48] using the FDTD were employed.

$$\nabla \times \left(\frac{1}{\varepsilon(r)} \nabla \times H(r)\right) = \left(\frac{\omega}{c}\right)^2 H(r) \tag{11}$$

$$\nabla \times \nabla \times E(r) = \left(\frac{\omega}{c}\right)^2 \varepsilon(r) E(r) \tag{12}$$

$$H_x^{n+\frac{1}{2}}\left(i, j+\frac{1}{2}\right) = H_x^{n-1/2}(i, j+1/2) - \frac{\Delta t}{\mu_0}\left[\frac{E_z^n(i, j+1) - E_z^n(i, j)}{\Delta y}\right]$$

$$H_y^{n+1/2}(i+1/2, j) = H_y^{n-1/2}(i+1/2, j) - \frac{\Delta t}{\mu_0}\left[\frac{E_z^n(i+1, j) - E_z^n(i, j)}{\Delta x}\right]$$

$$E_z^{n+1}(i, j) = E_z^n(i, j) + \frac{\Delta t}{\varepsilon_0 \varepsilon(i.j)}\left[\frac{H_y^{n+\frac{1}{2}}\left(i+\frac{1}{2}, j\right) - H_y^{n+\frac{1}{2}}\left(i-\frac{1}{2}, j\right)}{\Delta x} - \frac{H_x^{n+\frac{1}{2}}\left(i, j+\frac{1}{2}\right) - H_x^{n+\frac{1}{2}}\left(i, j-\frac{1}{2}\right)}{\Delta y}\right] \tag{13}$$

3. DESIGN OF THE PC BIOSENSOR

2-D photonic crystal structure planned in this research includes of a square lattice of rods of GaAs in SiO2. PhC structure has a lattice constant a = 410nm,

and a rods radii of 0.182a. The refractive indices of GaAs and SiO2 are nearly 3.8 and 1.46 respectively at a wavelength of 1.55 μm.

The proposed structure that mentioned in this article consists of a micro-cavity and two waveguides. Two waveguide couplers are provided with omitting some rods of central row. These waveguides are applied to couple the light to the cavity properly. The cavity is also obtained by etching the center of SiO2. The inlet and outlet waveguides and the cavity are separated by some rods.

Incorporating by PC waveguide, coupled micro-cavities obtain a handful of benefits due to compactness, high sensitivity, and quality factor. In fact, as one of the most important elements in the design of filters with a high transmission coefficient and Q factor, the cavity plays a significant role in improving the specifications of PC sensors. To calculate the band-gap, two-dimensional PWE were used. The diagram shows a TE band-gap, and there is no magnetic field to propagate. The proposed structure has a TE-polarized band-gap in 1269 nm-1565 nm, as shown in Fig.2.

To analyze the transmission spectra of the proposed structure, two-dimensional FDTD, (2D FDTD) approach is applied. A gaussian light source with a wavelength of 1400nm was set at the head of input waveguide. We must not forget that bordering conditions in the spatial edges of the analytical area should be considered in our simulations. A spatial unit thick PML is used to absorb the field that leaves the structure to prevent reflections.

The computation area consists of a 17*15 matrix of rods and grid spacing is selected to be a/32 and all simulations are handled in the same resolution to provide results at the same conditions. Also, the time step Δt selected in the simulation must fulfill the following stability equation.

$$\Delta t \leq \frac{1}{c} \times \frac{1}{\sqrt{\Delta x^{-2} + \Delta y^{-2}}} \quad (14)$$

The structure of the proposed biosensor and the electric field distribution are illustrated in Fig.3 and Fig4. The first step in designing a biosensor is to have a high Q-factor and transmission coefficient. Fig.5 shows the dependence of the Q-factor and the transmission spectrum on the number of rods (N) between the cavity and the two waveguides that changes from 1 to 3 when the cavity radius is 0.55a. First, the Q-factor increases with increasing the number of rods and reaches a maximum value of 145 for N=2. Then, it drops to 105 for N = 3. Also, when the number of rods increases from one to three, the amplitude of the transmission spectrum of the PC structure decreases slowly. After that, it decreases substantially. The optimal Q-factor and transmission coefficient values for the structure with N = 2 rods reach 145 and 61.5%, respectively. These are acceptable results for the design.

Another parameter affecting sensitivity is the micro-cavity radius. In this paper, a radius greater than 0.5a was chosen from the beginning. The main reason for choosing a micro-cavity with a large radius is to limit the effect of dimensions and lithography error on the sensitivity.
The dependence of the Q-factor and the transmission spectrum on the micro-cavity radius is shown in Fig.6. The cavity radius range has been considered from 0.5a to 0.65a. As the figure shows, the optimum value cavity radius is 0.6a. At this point, a transmission coefficient of 0.65 and a Q-factor of 155 were obtained. Fig.7 illustrates the sensor transmission spectrum after optimization and applying the Gaussian source with a wavelength of 1.4µm. The figure illustrates that the resonance wavelengths for healthy and cancerous basal cells are 1.3781µm and 1.3911µm, respectively. It is due to the fact that this structure creates a strong light field inside the cavity that enables it to be very sensitive to changes in refractive index due to the combination of light and matter. A 13 nm shift of the transmission spectrum wavelength between healthy and cancerous cells means the sensor sensitivity of 650.

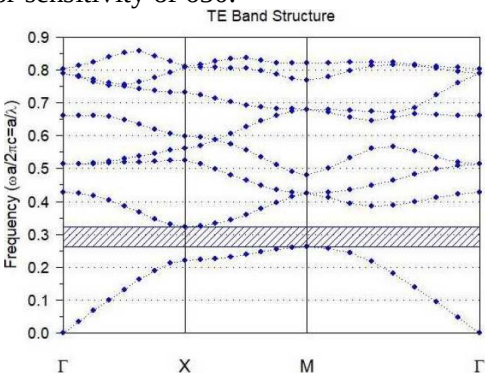

Fig. 2. The proposed biosensor band structure

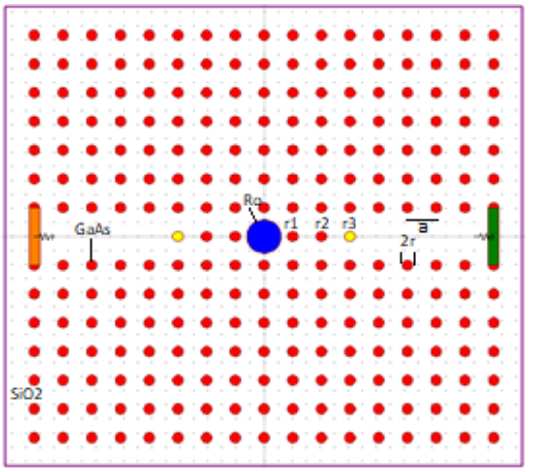

Fig. 3. The structure of the designed biosensor

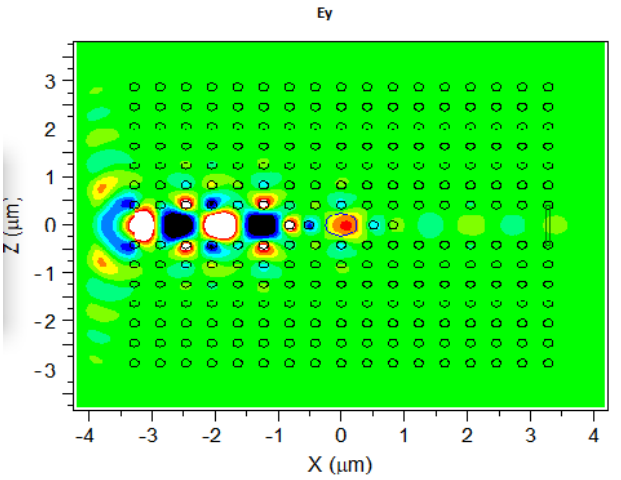

Fig. 4. The biosensor electric field distribution

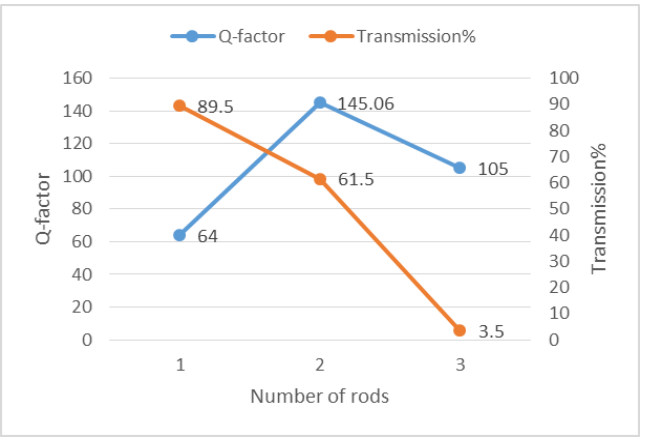

Fig. 5. The transmission spectrum and Q-Factor in terms of the number of rods (N).

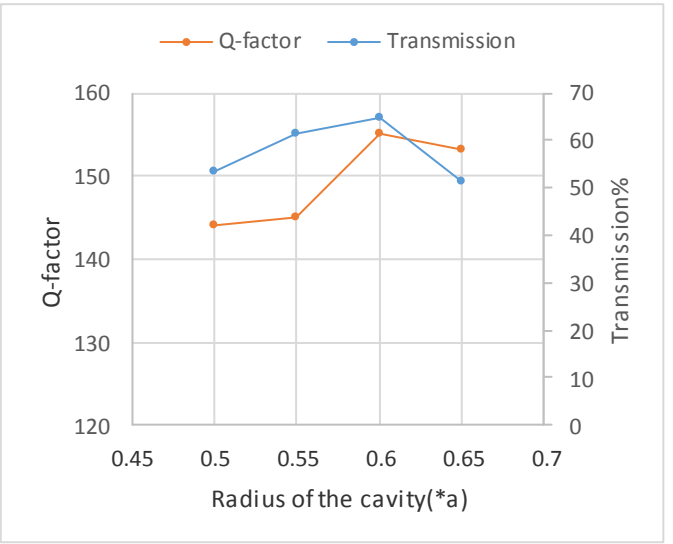

Fig. 6. The Q-factor and Transmission versus the cavity radius (from 0.5a to0.65a).

4. OPTIMIZATION OF THE PROPOSED SENSOR

For optimizing the sensitivity and Q-factor of the suggested design, the radius of two rods between the cavity and two waveguide couplers are changed with adjusting radius and location of r1, r2. The structure of optimized biosensor was indicated in Fig.8. We fixed the amount of cavity radius (Ro) in 0.6a, and, the location and radius of r1, r2 are changed relative to their values in the main

lattice (Fig.2). Radius of the rods and their displacements are firstly set as shown by amount of step number in Table I.

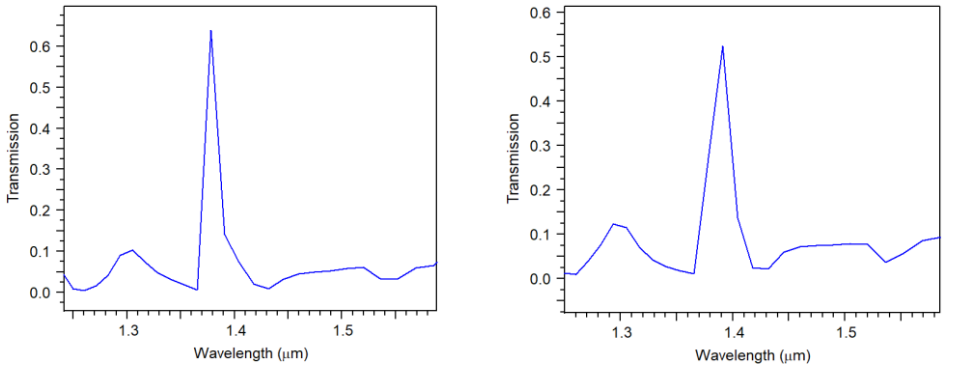

(a) (b)

Fig. 7. The spectra of the suggested sensor (a) for n= 1.36 and (b) for 1.38, the resonance wavelength have occurred in 1.3781μm and 1.3911μm respectively.

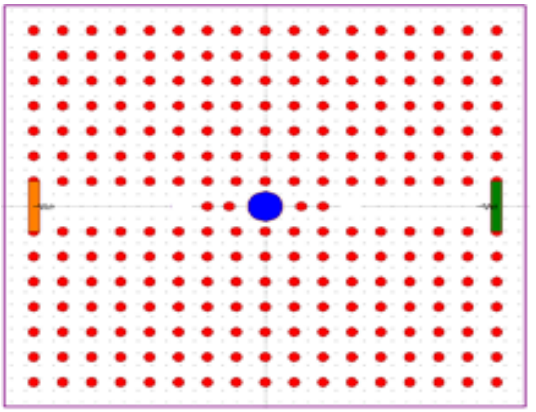

Fig. 8. The structure of the optimized biosensor

According to rows 1-3, the radius of r1 has been altered in the range of 0.9r to 1.1r with steps of 0.05r. The best value is shown in row 2. Then by keeping the value of r1 constant and altering the value of r2 in 0.05 steps, we get the values for this rod in rows 4 and 5. The best value for r2 is still obtained according to row 2. By keeping the optimal values for r1, r2 we changed the position of these rods in steps of 0.05a, and results are presented in rows 6-9. Finally, the best values of optimized design are shown in row 10.

As the above table indicates, the replacement of r1 plays a significant role in the resonance wavelength position. Hence, optimal values of r1 and r2 were both selected to be equal to ”r”, and ” r1s=0.25a” and ” r2s=0”.
r =74.6nm, and r1s and r2s are the amounts of displacement of r1 and r2 respectively, and the (+) sign indicates that the rod is away from the center of the structure, and the (-) sign indicates that the rod is approaching the center.

Fig.8 indicates the structure of the optimized biosensor. The numerical simulation due to the results of Table I is shown in Fig.9. As it is seen for n= 1.36, the resonance wavelength of transmission spectra occurred at 1.46μm. After filling the micro-cavity of the sensor with cancerous cell refractive index (n=1.38), due to receptor analyte interaction, a 14.6nm shift in resonance wavelength occurred, result in novel resonance wavelength reaches 1.4746μm. In fact, moving the rod in the waveguide causes irregularities in the path of the light, which itself causes more interaction between analyte and light, leading to a bigger change in resonant wavelength. The suggested design has a high sensitivity of 730 nm/RIU. Furthermore, the Q-factor of the sensor has been improved from 155 in the previous design to 161 in the optimized design. Moreover, the amplitude of normalized transmission spectra was improved from 0.65 to 0.89.

Table I
The process of optimization of transmittance coefficient, quality factor, and sensitivity in terms of radius and displacement of r1, r2.

step num-ber	r1 (×r)	r2 (×r)	r1s	r2s	Transm ission%	Q-Factor	Sensitivi-ty
1	0.9	1	0	0	51	162.5	640
2	1	1	0	0	65	155	650
3	1.05	1	0	0	86.6	154.5	635
4	1	0.9	0	0	71.7	71	645
5	1	1.05	0	0	59.5	160.2	647
6	1	1	0.2a	0	77	149	715
7	1	1	0.25a	0	89	161	730
8	1	1	0.27a	0	84	151	<700
9	1	1	0.25a	±0.05a	Not accept.	<150	<700
The best	1	1	0.25a	0	89	161	730

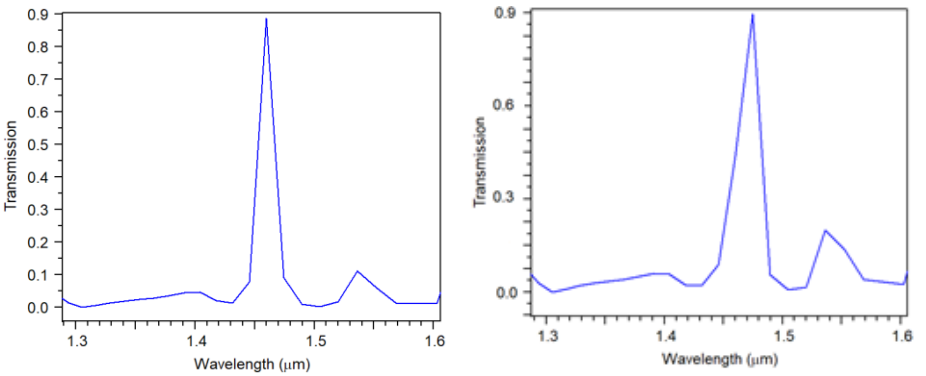

(a) (b)

Fig. 9. The transmission spectra of the optimized sensor (a) for n= 1.36 and (b) for n=1.38, the resonance wavelength has occurred in 1.46μm and 1.4746μm respectively.

5. COMPARISON

In this section, to compare the features of this sensor with other PC-based sensors having been designed in recent years, their characteristics are depicted in Table II. The table shows the various parameters of the sensors, including the sensitivity and the Q-factor of the sensors. By comparing the sensors, it is obvious that the sensitivity, as sensor's most important parameter, is higher than all the mentioned sensors. The output efficiency of the proposed sensor is also among the sensors that have the highest efficiency. However, the designed sensor does not have a very high Q-factor.

For commercial sensors, the maximum allowable Q factor depends on the manufacturing error tolerance. If the fabrication process is very precise, there is a limited frequency change.

This allows the use of higher Q-factor filters. Because a high Q-factor sensor is required to have an accurate manufacturing process, it increases the cost of the sensor.

6. SENSITIVITY AND FoM ANALYSIS

One of the essential characteristics of a sensor that should be considered in their design is that while the sensor sensitivity to the analyte refractive index should be high, its sensitivity to other structural parameters such as the rods' radii should be very low. In the manufacturing process, due to lithography error and manufacturing error, the dimensions of each structure component will be different from what was obtained in the design—reducing these errors increasing fabrication costs. This method is justified for designing laboratory sensors, while it is not justified for their commercialization. Therefore, it is very

important to design a sensor that, despite the manufacturing error, has minimum sensitivity to the sensor components. The different parameters of the designed sensor on sensitivity are investigated, and the sensitivity values are calculated.

Table II

Comparison between the suggested sensor features and some other PC biosensor

Ref.	Year	Mechanism	Sensitivity	Q-factor	Lattice	substrate
[49]	2009	Phc *Nano ring resonator*	5	>2000	Hexagonal lattice of water holes	Si plate
[50]	2013	Phc *Nano ring resonator*	165.45	4000	A hexagonal array of holes	SOI
[51]	2013	*Nano cavity resonator*	65.7	4793.6	Hexagonal lattice of air holes	Si slab
[52]	2014	Phc *Nano ring resonator*	Not mentioned	Not mentioned	Hexagonal lattice of holes	Si plate
[53]	2014	Phc micro-cavity	141.67	15000	Hexagonal lattice of air holes	Si slab
[40]	2016	Phc nano-cavity	391	4870	Hexagonal lattice of rods in air	SOI
[43]	2018	Phc *ring resonator*	690	2500	a square lattice of pillar-like rods	Si slab
[54]	2019	Phc n*an cavity*	473.78	6044.5	Hexagonal lattice of rods on air	-
[18]	2019	quasi-PC ring micro-cavity	613	79423	Stampfli-type of air holes	Si
[5]	2019	Phc *ring shape cavity*	300	418	Hexagonal lattice of air holes	Si slab
This work	2020	Phc micro-cavity	730	161	A square array of GaAs rods in SiO2	GaAs

The first parameter to be investigated is the role of rods' radii changes in the frequency shift of the transmission spectrum. This dependency is shown in Fig.10. In this figure, the radii of the rods are changed around the optimal point (r=74.6nm), and its effect on the resonance wavelength displacement and consequently the sensitivity to it are measured ($S_r=\partial\lambda/\partial r$). As the diagram

shows, the rods' radii change from 71 to 77 nm, while the sensitivity changes by the value of 0.3nm. By plotting the fit curve, the sensitivity of the biosensor to rods' radii around the optimal point is obtained at 0.063.

Another parameter that may affect the sensitivity is the cavity radius that emerged inside the structure. As aforementioned, at the beginning of the design, we chose a large radius cavity to reduce the effect of its dimensions on the sensitivity and the lithography error. However, by changing the cavity radius in the range of 0.55a to 0.65a nm, the sensitivity behavior to this parameter ($S_{RO}=\partial\lambda/\partial RO$) is shown in Table III. It indicates the relationship between micro-cavity radius and resonance wavelength, and Q-factor. As predicted, Table III confirms that by changing 0.1a (41 nm) in the radii of the cavity, the resonance wavelength does not change. However, it reduces the Q-factor a little, that it is negligible. In these calculations, we consider the refractive index to be 1.36.

Table III shows that the resonance wavelength remains unchanged due to the above changes in the cavity radius .Therefore, changing the cavity radius around the designed point does not affect the sensitivity of the sensor. The location of the micro-cavity and its displacement from the center of the structure may be another parameter affecting the shift of the resonance wavelength. Fig.11 illustrates the dependence of the transmission spectra on the displacement of the cavity. In this figure, the cavity center is displaced in the range of -0.07a to 0.07a relative to the original location. As shown, in the above range ($\pm 28nm$), the sensor's sensitivity to the displacement of the cavity remains unchanged; however, the output efficiency decreases to 0.86. Table IV shows complete information on the dependence of the transmission spectrum on the displacement of the cavity.

Fig. 12 illustrates the relationship between the resonance wavelength shift (λ_{res} (n=1.38) - λ_{res} (n=1.36)) and the cavity displacement. It shows that by changing the position of the cavity, the wavelength's difference remains constant.

Table IV and figures 11, 12 show that the resonance wavelength remains unchanged due to the changes in the cavity displacement .Therefore, changing the cavity displacement around the designed point does not affect the sensitivity of the sensor.

Now we define the figure of merit (FoM) parameter in the following form:

$$FoM=\frac{Sn}{\sqrt{\left(S_r^2+S_{R_0}^2+S_{sR_0}^2\right)}} \quad (15)$$

S_r and S_{RO} are the sensitivity of the resonance wavelength displacement to

The rods' radii and to the radius of the cavity respectively. Also, S_n is the sensitivity of the biosensor.

Based on the above relation, the FoM of the suggested sensor is 11428.

Because in this paper we were able to confine the spatial profile of the resonant state in the cavity where the analyte changes. Due to (2), it will enhance$\Delta\omega/\omega res$. To increase the sensor's sensitivity to analyte refractive indices, either $\Delta\omega/\omega res$ or Q-factor has to be incremented. As previously noted, due to the limitation of the Q-factor, we should try to enhance$\Delta\omega/\omega res$. The spatial resonance profile, which is greatly confined within the cavity, obtains a large $\Delta\omega/\omega res$ for a small refractive index changes.

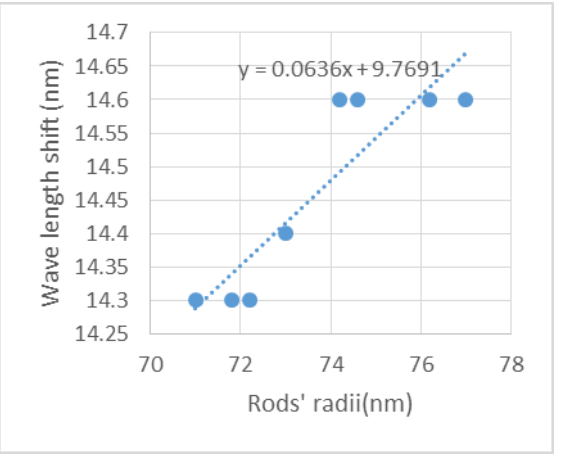

Fig. 10. The role of rods' radii in the wavelength shift (λ_{res} (n=1.38) - λ_{res} (n=1.36)) of the transmission spectra.

Table III
The relationship between micro-cavity radius and resonance wavelength (λ_{res} (n=1.36)) and Q-factor for n=1.36.

value of cavity radius(Ro)	resonance wavelength	Q-factor
0.55a	1.46	152
0.575a	1.46	156
0.6a	1.46	161
0.625a	1.46	159
0.65a	1.46	158

Table IV
The dependence of the transmission spectrum on the displacement of the cavity.

value of the cavity displacement (RoS) (nm)	**resonance wavelength (μm) (λ_{res} (n=1.36))**	**Transmission**
±0.07a	1.46	0.86
±0.05a	1.46	0.87
±0.03a	1.46	0.876
±0.01a	1.46	0.885
0	1.46	0.89

The above results show that the designed sensor has very little sensitivity to the structure parameters, and at the same time, its sensitivity to changes in the analyte refractive index is about 730nm/RIU.

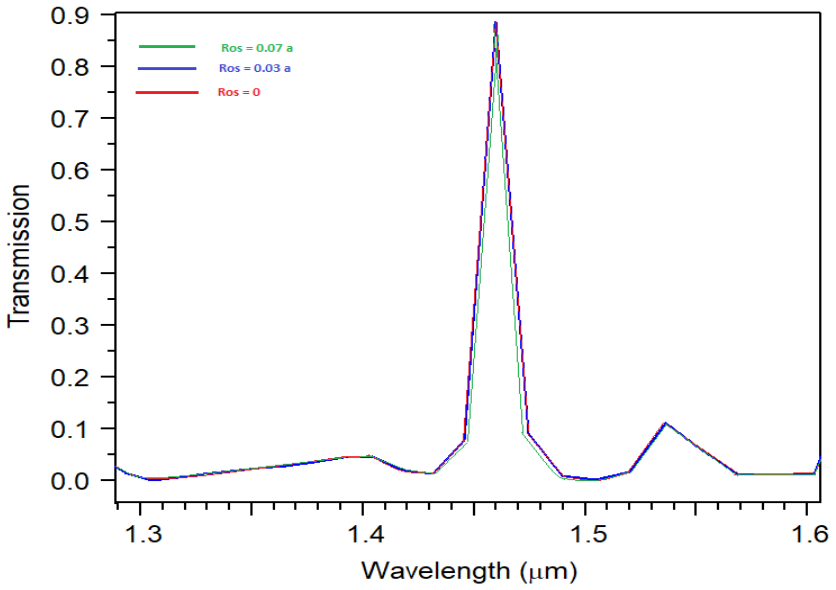

Fig. 11. The transmission spectra versus of the displacement of the cavity for n=1.36

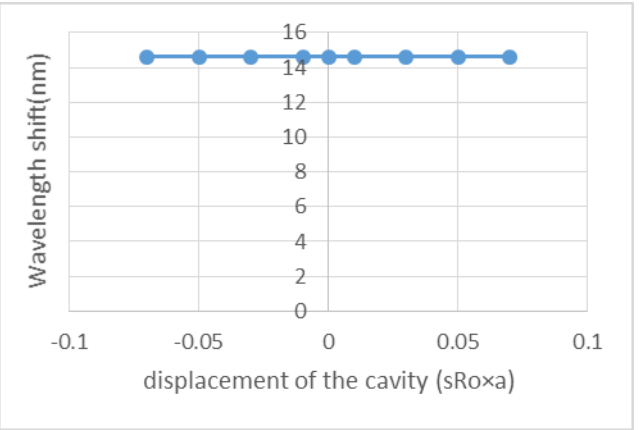

Fig. 12. The dependence of the wavelength shift (λ_{res} (n=1.38) - λ_{res} (n=1.36)) on the displacement of the cavity.

7. CONCLUSION

A novel 2D PC-based refractive index sensor was suggested. The structure involves a square lattice of GaAs rods in SiO2. It is formed by one micro-cavity and two waveguide couplers. Two waveguide couplers are provided by removing many rods of one row in the x-direction. They are utilized to couple lights to the micro-cavity. The micro-cavity is provided by etching of SiO2 in the PC structure center (Ro = 0.6a). Some rods have separated the cavity from two PC waveguides.

To optimize the sensor's sensitivity, we altered the cavity radius and rod's radii located between two line defects and micro-cavity, also we altered the distance between rods and cavity. For sensing aims, a refractive index measurement structure is applied in which the resonance wavelength shifts by changing the micro-cavity refractive index. It has resulted in a displacement in transmission spectrum resonant wavelength.

The structure was numerically simulated, and it was indicated that sensitivity and transmission efficiency of the refractive index sensor could be reached 730nm/RIU and 89% respectively when r = 0.182a.

In the designed sensor, the resonant wavelengths for refractive indexes of 1.36 and 1.38 are obtained at λ_{res} = 1.46μm and λ_{res} = 1.4746μm respectively. Therefore, the suggested compact, robust, and high- sensitivity PhC micro-cavity sensor array with a high FoM is an ideal platform to realize highly RI sensing.

REFERENCES

[1] J.D.Joannopoulos, P.R. Villeneuve, and S. Fan. *Erratum: Photonic crystals: putting a new twist on light.* Nature. [online]. 387(6635) (1997, March) 830-830. Available: https://www.nature.com/articles/386143a0

[2] Q.Yan, L. Wang, and X.S. Zhao. *Artificial Defect Engineering in Three-Dimensional Colloidal Photonic Crystals.* Advanced Functional Materials. [online]. **17**(18) (2007, Nov.) 3695-3706. Available: https://doi.org/10.1002/adfm.200600538

[3] C.-C. Wang, and L.-W. Chen. *Channel drop filters with folded directional couplers in two-dimensional photonic crystals.* Physica B: Condensed Matter. [online]. 405(4) (2010, Feb.) 1210-1215. Available: https://doi.org/10.1016/j.physb.2009.11.044

[4] B. Saghirzadeh Darki, and N. Granpayeh. *Improving the performance of a photonic crystal ring-resonator-based channel drop filter using particle swarm optimization method.* Optics Communications. [online]. 283(20) (2010, Oct.) 4099-4103. Available: https://www.sciencedirect.com/science/article/abs/pii/S0030401810006073

[5] M. Lee, and P.M. Fauchet, *Two-dimensional silicon photonic crystal based biosensing platform for protein detection.* OPTICS EXPRESS. [online]. 15(8) (2007, Apr.) 4530-4535. Available: https:// DOI: 10.1364/OE.15.004530

[6] M.Djavid, and A.M. Ghaffari, and M.S.Abrishmian. *Photonic_Crystal_Narrow_Band_Filters_Using Biperiodic Structures.* Journal of Applied sciences. [online]. 8(10) (2008) 1891-1897. Available: https://scialert.net/fulltext/?doi=jas.2008.1891.1897&org=11

[7] S. Robinson, and r. Nakkeran. *Investigation on Photonic Crystal based Filter using Square, Circular and Hexagonal rods.* International Conference on Computer, Communication and Electrical Technology – ICCCET. [online]. (2011, March). Available: https://ieeexplore.ieee.org/abstract/document/5762485

[8] Z. Qiang and W. Zhou. *Optical add-drop filters based on photonic crystal ring resonators.* OPTICS EXPRESS. [online]. 15(4) (2007, Feb.) 1823-1831. Available: https://opg.optica.org/oe/abstract.cfm?uri=OE-15-4-1823

[9] J.J.V Olmos, M. Tokushima, and K.I. Kitayama. *Photonic Add–Drop Filter Based on Integrated Photonic Crystal Structures.* IEEE Journal of Selected

Topics in Quantum Electronics. [online]. 16(1) (2010, Jan.) 332-337. Available: https://**doi:** 10.1109/JSTQE.2009.2028901

[10] P. Andalib, and N. Granpayeh, *Optical Add/drop Filter Based on Dual Curved Photonic Crystal Resonator. IEEE/LEOS International Conference on Optical MEMs and Nanophotonics*. [online]. (2008, Aug.). Available: https://**doi:** 10.1109/GROUP4.2008.4638161

[11] F. Monifi, and A.G.M. Djavid, and M.S. Abrishamian. *A_New_Bandstop_Filter_Based_on_Photonic_Crystals.* Progress In Electromagnetics Research Symposium. [online]. (2008, July) 674-677. Available: https://www.researchgate.net/publication/266228117

[12] V. Fallahi , M.Seyfouri. *Novel Structure of Optical Add/Drop Filters and Multi-Channel Filter Based On Photonic Crystal for Using In Optical Telecommunication Devices.* Journal of Optoelectronical Nanostructures. [online]. 4(2) (2019, Nov.) 53-68. Available: http://jopn.miau.ac.ir/article_3478.html

[13] Z. Rashki, S.J.S.M.C., *Novel Design for Photonic Crystal Ring Resonators Based Optical Channel Drop Filter.*. Journal of Optoelectronical Nanostructures (JOPN). [online]. 3(3) (2018, Summer) 59-78, Available: http://jopn.miau.ac.ir/article_3046.html

[14] V. Fallahi, M.Seyfouri. *Design of an Improved Optical Filter Based on Dual-Curved PCRR for WDM Systems.* Journal of Optoelectronical Nanostructures (JOPN). [online]. 2(3) (2017, Autumn) 45-56. Available: http://jopn.miau.ac.ir/article_2573.html

[15] Q. Gong, and X. Hu, Photonic photonic crystal sensors, in *Photonic Crystals: Principles and Applications*, Taylor & Francis Group, Pan Stanford publishing, 2014, 336-340, Available: https://api.taylorfrancis.com/content/books/mono/download?identifierName=doi&identifierValue=10.1201/b15654&type=googlepdf

[16] R.V. Nair, and R. Vijaya. *Photonic crystal sensors: An overview.* Progress in Quantum Electronics. [online]. 34(3) (2010, May) 89-134. Available:https://doi: 10.1016/j.pquantelec.2010.01.001

[17] M. Danaie, and B. Kiani. *Design of a label-free photonic crystal refractive index sensor for biomedical applications.* Photonics and Nanostructures - Fundamentals and Applications. [online]. 31 (2018, Sep.) 89-98.

Available:https://doi: 10.1016/j.photonics.2018.06.004

[18] A. Shi, R. Ge, and J. Liu. *Refractive index sensor based on photonic quasi-crystal with concentric ring microcavity.* Superlattices and Microstructures. [online]. 133 (2019, Sep.) 106198.

Available: https://doi.org/10.1016/j.spmi.2019.106198

[19] S. Mandal, and D. Erickson. *Nanoscale optofluidic sensor arrays.* Optics Express. [online]. 16(3) (2008, Jan.) 1623-1631.

Available:https://doi: 10.1364/OE.16.001623

[20] V. Fallahi , M.Seifouri. *Novel Four-Channel All Optical Demultiplexer Based on Square PhCRR for Using WDM Applications.* Journal of Optoelectronical Nanostructures. [online]. 3(4) (2018, Autumn) 59-70. Available: http://jopn.miau.ac.ir/article_3262.html

[21] S. M. Hosein, M.S. Jalali, G. Akbarizadeh, *Ultra-fast 1-bit comparator using nonlinear photonic crystalbased ring resonators.* [online]. 4(3) (2019, Autumn) 59-72, Available: http://journals.miau.ac.ir/article_3620.html

[22] J.D. Joannopoulos, et al, *molding the flow of light*, in *Photonic crystals*, 2nd. Edition, *Princeton University Press; 2008*, Available: https://www.amazon.com/Photonic-Crystals-Molding-Light-Second/dp/0691124566

[23] Y. Tsuji, Y. Morita, and K. Hirayama. *Photonic Crystal Waveguide Based on 2-D Photonic Crystal With Absolute Photonic Band Gap.* IEEE Photonics Technology Letters. [online]. 18(22) (2006, Nov.) 2410-2412.

Available: https://doi: 10.1109/lpt.2006.885295

[24] F.-l. Hsiao, and C. Lee. *Computational Study of Photonic Crystals Nano-Ring Resonator for Biochemical Sensing.* IEEE Sensors Journal. [online]. 10(7) (2010, July) 1185-1191.

Available:https:// doi**:** 10.1109/JSEN.2010.2040172

[25] E. Chow, et al. *Ultracompact biochemical sensor built with two-dimensional photonic crystal microcavity.* Optics Letters. [online]. 29(10) (2004, May) 1093-1095. Available: https://opg.optica.org/ol/abstract.cfm?uri=OL-29-10-1093

[26] C. Caër, et al. *Liquid sensor based on high-Q slot photonic crystal cavity in silicon-on-insulator configuration.* Optics Letters. [online]. 39(20) (2014,

Oct.) 5792-5794. Available: https://opg.optica.org/ol/abstract.cfm?uri=ol-39-20-5792

[27] A. Benmerkhi, M. Bouchemat, and T. Bouchemat. *Improved sensitivity of the photonic crystal slab biosensors by using elliptical air holes.* Optik. [online]. 127(14) (2016, july) 5682-5687.

Available:https://doi.org/10.1016/j.ijleo.2016.03.057

[28] S. Zlatanovic, et al. *Photonic crystal microcavity sensor for ultracompact monitoring of reaction kinetics and protein concentration.* Sensors and Actuators B: Chemical. [online]. 141 (2009, Aug.) 13-19.

Available:https://doi: 10.1016/j.snb.2009.06.007

[29] M. Lee , and P.M. Fauchet. *Two-dimensional silicon photonic crystal based biosensing platform for protein detection.* Optics Express. [online]. 15(8) (2007, Apr.) 4530-4535. Available: https://doi: 10.1364/OE.15.004530

[30] H.S. Dutta, and S. Pal. *Design of a highly sensitive photonic crystal waveguide platform for refractive index based biosensing.* Optical and Quantum Electronics. [online]. 45(9) (2013, May) 907-917.

Available:https://link.springer.com/article/10.1007/s11082-013-9697-x

[31] H.S. Dutta, A.K. Goyal, and S. Pal. *Sensitivity enhancement in photonic crystal waveguide platform for refractive index sensing applications.* Journal of Nanophotonics. [online]. 8(1) (2014, Jun.) 083088. Available: https://doi.org/10.1117/1.JNP.8.083088

[32] Y.-n. Zhang,., Y. Zhao, and Q. Wang. *Multi-component gas sensing based on slotted photonic crystal waveguide with liquid infiltration.* Sensors and Actuators B: Chemical. [online]. 184 (2013, Jul.) 179-188. Available: https://doi.org/10.1016/j.snb.2013.04.082

[33] A. Harhouz, and A. Hocini. *Design of high-sensitive biosensor based on cavity-waveguides coupling in 2D photonic crystal.* Journal of Electromagnetic Waves and Applications. [online]. 29(5) (2015, March) 659-667. Available: https://doi: 10.1080/09205071.2015.1012597

[34] X .Wang, et al. *Ultracompact refractive index sensor based on microcavity in the sandwiched photonic crystal waveguide structure.* Optics Communications - OPT COMMUN. [online]. 281 (2008, March) 1725-1731. Available: https://doi: 10.1016/j.optcom.2007.11.040

[35] X. Wang, et al. *Photonic crystal refractive index sensing based on sandwich structure.* Optik. [online]. 123(23) (2012, Dec.) 2113-2115 https://doi.org/10.1016/j.ijleo.2011.10.008

[36] A. Hocini, and A. Harhouz. *Modeling and analysis of the temperature sensitivity in two-dimensional photonic crystal microcavity.* Journal of Nanophotonics. [online]. 10(1) (2016, Feb.) 016007.

Available:https://doi: 10.1117/1.jnp.10.016007

[37] D. Yang, H. Tian, and Y. Ji. *Nanoscale photonic crystal sensor arrays on monolithic substrates using side-coupled resonant cavity arrays.* Optics Express. [online]. 19(21) (2011, Sep.) 20023-20034.

Available: https://doi.org/10.1364/OE.19.020023

[38] L. Huang, et al. *Design low crosstalk ring-slot array structure for label-free multiplexed sensing.* Sensors (Basel). [online]. 14(9) (2014, Aug.) 15658-68. Available:https://doi: 10.3390/s140915658

[39] *S. Upadhyay, VL Kalyani. High sensitive refractive index sensor based on 2D-photonic crystal.* IJERT. [online]. 4 (2015, Feb.) 1006-1010. Available: https://www.ijert.org/high-sensitive-refractive-index-sensor-based-on-2d-photonic-crystal

[40] S. Jindal, et al. *Nanocavity-Coupled Photonic Crystal Waveguide as Highly Sensitive Platform for Cancer Detection.* IEEE Sensors Journal. [online]. 16(10) (2016, May) 3705-3710. Available: https://doi: 10.1109/jsen.2016.2536105

[41] M. Ammari, F. Hobar, and M. Bouchemat. *Photonic crystal microcavity as a highly sensitive platform for RI detection.* Chinese Journal of Physics. [online]. 56(4) (2018, Aug.) 1415-1419. Available:https://doi: 10.1016/j.cjph.2018.05.010

[42] F. Rahman-Zadeh, M. Danaie, and H. Kaatuzian. *Design of a highly sensitive photonic crystal refractive index sensor incorporating ring-shaped GaAs cavity.* Opto-Electronics Review. [online]. 27(4)(2019, Dec.) 369-377. Available: https://doi: 10.1016/j.opelre.2019.11.007

[43] A.Tavousi, M.R. Rakhshani, and M.A. Mansouri-Birjandi. *High sensitivity label-free refractometer based biosensor applicable to glycated hemoglobin detection in human blood using all-circular photonic crystal ring resonators.* Optics Communications. [online]. 429 (2018, Dec.) 166-174. Available: https://doi.org/10.1016/j.optcom.2018.08.019

[44] D.M. Pozar, *Microwave engineering*, 4th. ed., John wiley & sons, 2012, 6-15.

Available:https://www.wiley.com/en-ie/Microwave+Engineering,+4th+Edition-p-9780470631553

[45] M. Soljačić, et al., *Photonic-crystal slow-light enhancement of nonlinear phase sensitivity*. Journal of the Optical Society of America B, [online]. 19(9) (2002, Sep.) 2052-2059, Available: https://doi: 10.1364/JOSAB.19.002052

[46] K.M. Leung, and Y.F. Liu. *Photon band structures: The plane-wave method*. Physical Review B. [online]. 41(14) (1990, May) 10188-10190. Available:https://doi: 10.1103/PhysRevB.41.10188

[47] K.M. Ho, C.T. Chan, and C.M. Soukoulis. *Existence of a photonic gap in periodic dielectric structures*. Physical Review Letters. [online]. 65(25) (1990, Dec.) 3152-3155. Available: https://journals.aps.org/prl/abstract/10.1103/PhysRevLett.65.3152

[48] T.S. Mostafa, N.A. Mohammed, and E.-S.M. El-Rabaie. *Ultracompact ultrafast-switching-speed all-optical 4 × 2 encoder based on photonic crystal*. J. Comput. Electron. [online]. 18(1) (2019, Nov.) 279–292. Available: https://link.springer.com/article/10.1007/s10825-018-1278-6

[49] F.-L. Hsiao, and C. Lee. *Novel Biosensor Based on Photonic Crystal Nano-Ring Resonator*. Procedia Chemistry. [online]. 1(1) (2009, Sep.) 417-420. Available:https://doi.org/10.1016/j.proche.2009.07.104

[50] S. Olyaee, and S. Najafgholinezhad. *Computational study of a label-free biosensor based on a photonic crystal nanocavity resonator*. Applied Optics. [online]. 52(29) (2013, Oct.) 7206 Available: https://doi.org/10.1364/AO.52.007206

[51] S. Olyaee, S. Najafgholinezhad, and H. Alipour Banaei. *Four-channel label-free photonic crystal biosensor using nanocavity resonators*. Photonic Sensors. [online]. 3(3) (2013, Feb.) 231-236. Available:https://doi: 10.1007/s13320-013-0110-y

[52] S. Olyaee, and A. Mohebzadeh-Bahabady. *Designing a novel photonic crystal nano-ring resonator for biosensor application*. Optical and Quantum Electronics. [online]. 47(7) (2014, Nov.) 1881-1888.

Available:https://doi: 10.1007/s11082-014-0053-6

[53] S. Najafgholinezhad, and S. Olyaee. *A photonic crystal biosensor with temperature dependency investigation of micro-cavity resonator*. Optik. [online]. 125(21) (2014, Nov.) 6562-6565.

Available:https://doi: 10.1016/j.ijleo.2014.08.043

[54] N.A. Mohammed, et al. *High-sensitivity ultra-quality factor and remarkable compact blood components biomedical sensor based on nanocavity coupled photonic crystal*. Results in Physics. [online]. 14 (2019, Sep.) 102478. Available: https://doi.org/10.1016/j.rinp.2019.102478